Heliyon 11 (2025) e42420

Contents lists available at ScienceDirect

Heliyon

journal homepage: www.cell.com/heliyon

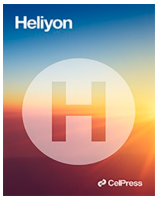

Research article

Mechanical characterization and testing of multi-polymer combinations in 3D printing

Ana María Gómez Amador *, Ricardo Andre Venturini Avendano, Alejandro Quesada González, Leopoldo Prieto Fernández

Universidad Carlos III de Madrid, Spain

ARTICLE INFO

Keywords:
3D printing
PLA
PETG
ABS
ASA
Industry 4.0
Gyroid

ABSTRACT

One of the key advancements brought on by Industry 4.0 is additive manufacturing, particularly material extrusion printers that enable the creation of complex parts using composite materials. This article presents a study on the mechanical behavior of 3D printing multi-materials, which are easily accessible and cost-effective for users. Tensile, compression, and flexural tests were conducted on various material configurations to explore their mechanical properties. Results indicate that certain material combinations exhibit enhanced properties in tension and compression, while individual materials perform stronger in flexural tests due to improved interlayer adhesion.

The research highlights how material combinations in 3D printing can impact the mechanical properties of parts, offering potential applications in structural design. The study found that a combination of PETG and PLA yields optimal mechanical properties in tensile tests, while configurations with PLA on the outer layer perform best in compression tests. It also identifies a limitation in flexural testing dimensions, where specimens with a 4 mm thickness restrict the possibilities of material combination tests.

1. Introduction

3D printing is a process for manufacturing a three-dimensional object from a computer-aided design (CAD) model. It consists of depositing molten material, usually layer by layer, solidifying it and creating the desired object. The advances that this technology is experiencing are enabling the use of materials that improve the properties of the printed parts.

There are different types of additive manufacturing technologies in 3D printing, the most common are: stereolithography (SLA), selective laser sintering (SLS), 3D printing (3DP), fused deposition (FDM). For the analyses and results presented in this article, the fused deposition modeling (FDM) has been used because it is considered the economical and accessible form of printing at the domestic level (as well as for industrial use).

Fused deposition modeling is based on the addition of material layers by extrusion through a heated steel nozzle. The material, through a computer model that breaks down the part into layers, is placed on a heated build bed and is added layer by layer until the part is finished [1]. FDM technology uses thermoplastic materials, because it is a technique where the temperature in the extruder is slightly above the melting temperature.

The use of FDM printers is the most widespread in general. Statistical studies conducted by Placek [2] on more than 1900 3D printer

* Corresponding author.
E-mail address: amgomez@ing.uc3m.es (A.M. Gómez Amador).

https://doi.org/10.1016/j.heliyon.2025.e42420
Received 1 September 2024; Received in revised form 30 January 2025; Accepted 31 January 2025
Available online 31 January 2025
2405-8440/© 2025 The Authors. Published by Elsevier Ltd. This is an open access article under the CC BY-NC-ND license (http://creativecommons.org/licenses/by-nc-nd/4.0/).

users reveal that more than 60 % of the respondents make use of an FDM printer from home versus the other technologies, for which their use is delegated to external companies. The cost of access to an FDM 3D printer is low and, at a technical level, its use is simple.

FDM is very useful in industry for rapid prototyping (RP). It enables designers to verify and correct their designs at very low costs. However, this technology is limited in other areas where the use of thermoplastics does not provide mechanical properties suitable for industries that need to withstand high loads, such as aeronautics and automotive [3]. For these applications, it is necessary to conveniently modify the printing parameters to achieve an isotropic part, which will improve the mechanical properties as much as possible without being limited by the material [4].

The use of better materials, such as composites, means an improvement in the mechanical properties of the material. However, the performance of a part depends not only on the manufacturing material itself, but also on aspects related to the printing of the part [5]. Such aspects are known as the printing parameters; these parameters are related to the material deposition rate, infill density, infill pattern, and layer height.

As for the printing parameters studied in this article, infill density, which limits the amount of material to use in the design, is the parameter that determines the weight and printing time. Therefore, it also dictates for the most part the cost of the part, which makes it a critical parameter to work with in printing. Infill density also influences the mechanical properties of the printed part, as demonstrated by Lennert et al. [6] when measuring the influence of density on the impact strength of parts. Lennert et al. [6] concludes that increasing the density also increases the impact strength by up to 46.67 %.

On the other hand, the infill pattern is the parameter with the greatest influence on the mechanical properties of the printed part. When defining an infill pattern, it should be considered which one distributes the stresses in a more isotropic way and has the lowest percentage of volume. According to the work done by Akhoundi [7], the triangular infill pattern presents the best tensile strength, while the honeycomb pattern obtains the lowest results.

The orientation in the impression of the part is another important and studied factor. This is because depending on the angle or position of the specimen, the results can vary. For example, when specimens are printed flat and on edge, they have up to 154 % better tensile strength than when printed vertically. The same is true for the angle at which this orientation is printed [8].

The materials studied in this article represent the most common materials in the domestic 3D printing environment. These materials are Polylactic Acid (PLA), Acrylonitrile Butadiene Styrene (ABS), Acrylonitrile Styrene Acrylate (ASA) and Polyethylene Terephthalate Glycol (PETG). Table 1 shows the properties of the materials used in this study.

PLA is one of the most widely used materials with FDM printers. Its low cost and good mechanical properties make it suitable for parts, with a tensile strength of up to 60 MPa [9] while also being biodegradable. On the other hand, it has low heat resistance, it starts to degrade from 50 C°, so it is not suitable for prints with high thermal stresses [10]. Another of the most commonly used materials is ABS, known for its hardness and impact resistance, which allows the parts to last through time and use. The printing process with this material requires ventilation systems as it emits harmful gases [11]. The ASA material has mechanical properties similar to ABS with the difference that it has UV resistance and good environmental stability. According to Raam et al. [12], ABS has excellent interlayer adhesion which gives it high impact resistance, durability, and good mechanical strength. Finally, PETG is a copolymer notorious for its high chemical resistance, biocompatibility, transparency, high impact resistance and for being easily recyclable [13]. It has different applications in the field of medicine, electronics and, being biocompatible, in the food field with an acceptable degree of flammability [14].

Once the materials to be used and the type of printer have been analyzed, it is necessary to study the feasibility of bonding the materials by physical/chemical means to analyze the behavior of their mechanical properties and whether they manage to compensate for the shortcomings in the bonding of one material to another. The focus of this paper is to study whether the behavior and bonding of the materials has isotropic characteristics and whether the adhesion between them is strong enough to resist a variety of loads. The printer used to manufacture the multi-material parts used in this study was the Prusa i3 MK3S multi-material printer (Fig. 1) with single nozzle filament selection system. These types of printers are preprogrammed with the materials to be used in a print and make use of a deposition tower for the change of filament prior to depositing on the hot bed of the printer [15].

The process of manufacturing with different materials is called multi-material additive manufacturing (MMAM). Manufacturing parts with different materials allows taking advantage of their different mechanical properties, but at the same time poses a challenge to current manufacturing methods [16]. 3D printing brings this possibility closer with MMAM as it allows the freedom of layer-by-layer or particle-by-particle design of parts [17].

There are previous works where materials are mixed by means of a 3D printer. In the work done by Tian et al. [18], simultaneous extrusion of carbon fiber reinforcement and PLA through the printer nozzle was performed. This method provided the PLA with reinforcement, as is done in concrete structures, giving it a maximum flexural strength of 335 MPa and a flexural modulus of 30 GPa. Such combinations are promising for the automotive or aeronautical sector. In the work of Schweiger, J. et al. [19], scanned replicas of a patient are made for a 3D printed denture prosthesis. The process consists of employing multi-material printers to give more strength and natural esthetics to the person's denture. These procedures usually require several phases of implementation, but, with the

Table 1
Properties of the materials used [9–11].

Mechanical properties	PLA	PETG	ASA	ABS
Tensile strength	60 MPa	32.3 MPa	35 MPa	45 MPa
Tensile modulus	3.5 GPa	1.3 GPa	2.2 GPa	2.3 GPa
Charpy Impact	5 kJ/m^2	2.8 kJ/m^2	5 kJ/m^2	5.3 kJ/m^2

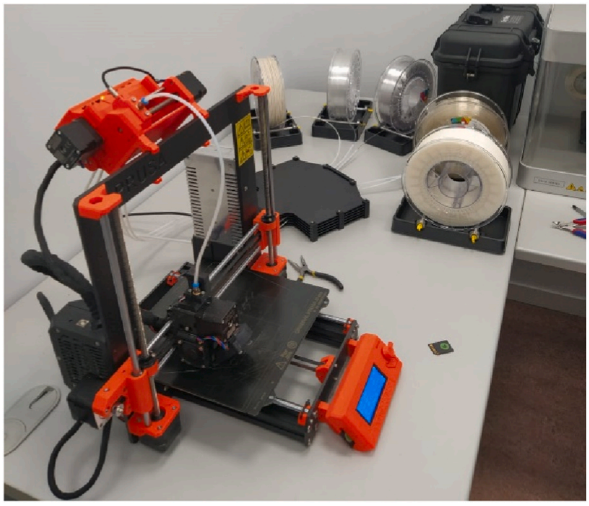

Fig. 1. Multifilament printer Prusa i3 MK3S & MK3S + MMUS.

harnessing of this technology, it is reduced to just one. Then, in the work of An. et al. [20], multi-material printing is performed with a combination of printing processes such as technology by dyes, powders in a procedure called "multi step 3D printing". The aim is to combine materials, adapting them to more complex and resistant structures with applications in the field of biomedicine. The adhesion of materials is supported by studies such as that of Yermurat et al. [21], who studied the bonding of PLA and ABS in tensile specimens in which better results were obtained with a substantial increase in tensile strength compared to those specimens made of a single material.

According to the literature review, previous authors have not analyzed the joining of materials using the gyroid pattern in fused deposition modeling printers. The contribution of this article is the characterization of certain material bonds and their properties, as well as the analysis of the mechanical behavior of the parts by varying their composition and printing patterns.

To carry out this characterization, mechanical tests (compression, tensile and flexural) were performed to study and analyze the behavior and properties of the materials. With the results obtained, it is possible to determine the influence of the mixtures of materials analyzed on the mechanical properties.

2. Printing methodology

a. Printing parameters

The printing parameters analyzed in this article are those that have a critical effect on the weight and printing shape of the part. The objective is to select an optimal infill pattern and infill density to obtain isotropy in mechanical properties. In this way, using a smaller amount of material (less weight) guarantees mechanical conditions similar to a 100 % solid specimen. Therefore, the infill pattern used in this article is the gyroid, which is characterized as a Triple Periodic Minimum Surface (TPMS) [22]. According to Qin et al. [23], the gyroid pattern presents one of the best strength-to-weight ratios. Qin tests a gyroid cube with graphene in compression and at a density of only 5 % compared to steel. When tested, the structure withstands 10 times the strength of steel. It is emphasized that the structure is the dominant factor in testing and can be used to design and predict the mechanical properties of a material. Other studies such as those of Vrana et al. [24] and Niam et al. [25] show that the gyroid pattern is better than other types of structures because it is rigid in all directions of space.

Regarding the infill density, it should be noted that the resolution allowed on the FDM printer used (Prusa i3 MK3S & MK3S + MMUS) is 0.05–0.3 mm with a 0.4 mm nozzle. This resolution is considered adequate considering that the strength of a part is limited by the size at which the walls are printed during printing. It is found that in small specimens there is a reduction in strength due to the size of the part compared to the part walls. However, large specimens are more constant with their strength by having walls in accordance with the dimension of the part [26]. This is also true according to Abueidda et al. [27] where deviations/impression defects were reduced at higher densities, thus resisting more, than in those specimens with low densities. These results are taking into account the limitations of the 3D printer. It is worth noting that at very high densities the geometric characteristics of the infill pattern are lost and could take away isotropy and therefore reduce its mechanical strength. This highlights the research of Bell, D., & Siegmund, T [26]. again since there must be a balance between part size and wall thickness to avoid loss in the structural characteristics of the TPMS.

According to later studies by Abbueida et al. [28], compression specimens were tested with densities of 7 %, 14 %, 30.5 %, 36 %, 40 % and 46 % and taking into account the conclusions of their previous study [27], at higher densities the isotropic effect of the gyroid would be lost which could cause specimen failure. The percentage with the highest compressive strength and lowest deformation was the 46 % density. From the stress-strain curves obtained by Abbueida et al. [28] it is found that the elastic zone deforms uniformly, in

high densities it was obtained that there is more uniform deformation compared to those low densities. Beyond the elastic zone, the low densities are more ductile but fluctuating in their deformation and become significantly stiffened, but not enough to overcome the high densities. Silva et al. [29] also concluded that the gyroid presents an improvement in mechanical strength with a density lower than 100 %. From the studies consulted, it can be ascertained that the gyroid pattern, together with a density of 46 %, are ideal for characterizing the material mixture in an FDM printer.

Silva et al. [29] also studies the influence of the perimeter walls of the impression and how they influence in improving the performance of the gyroid parameter, in their study they make use of 6 perimeter walls to leave enough space for the gyroid. The reason is that increasing the number of perimeter walls would mean sacrificing space for the infill pattern impression due to the high density of the specimen. These results agree with those obtained by Ćwikła et al. [30] where, in tests, but with bee infill pattern, Ćwikła [30] made specimens with 1, 2,4 and 7 perimeter walls, keeping the rest of the printing parameters constant (bee panel pattern, 40 % infill density). Starting from 4 perimeter walls in small areas, the infill pattern is reduced and replaced by grouped lines. This gives the material a solid behavior and a higher strength, similar to a 100 % sample density.

For the orientation of the specimens in the printing bed, according to the existing literature, the best properties are achieved at an angle of 0°. In this way the specimen fibers are arranged parallel to the load [8,31]. Also, for resolution and specimen dimensions, it was convenient to print aligned to the printing bed (Fig. 2) to ensure that the printer nozzle could shape the gyroid pattern. All other printing parameters are left with the default values of the slicing software, and, for the materials, the manufacturer's data sheets are used.

b. Used printer

Two different printers have been used, a multi-material Prusa i3 MK3S & MK3S + MMUS and another for single material specimens Prusa i3 MK2S both with a 0.4 mm diameter nozzle. The slicing software used is the default one that comes with the printers, the *PrusaSlicer*. The multifilament printer has a material distribution system (Fig. 3) through a single extruder. This system works with a laser sensor to distinguish the materials by their opacity and automatically makes the material exchanges according to the required layer. The printer makes use of a deposition tower (Fig. 4) and cleans the extruder as layers are made and material is changed. In other words, each material change requires a cleaning process of the single extruder which, although automated, takes approximately 20–45 s. During that interval the last printed layer cools down, which slightly reduces the adhesion between the newly deposited material and the previous layer. The reason for choosing a single-nozzle printer is that the authors want to apply the results of this research in a project for printing low-cost foot prostheses. For this reason, a basic multi-material printer that is readily available in developing countries has been selected.

The printer used for individual materials (Fig. 5) is the manufacturer's most commercial model and is suitable for printing with materials that emit toxic gases such as ABS.

c. Specimen configuration

To perform the three types of tests, three types of specimens have been designed: the tensile specimen in the shape of a bone, the compression specimen in the shape of a cylinder and the bending specimen in the shape of a rectangular prism.

For the tensile test, a bone-shaped specimen was designed according to the UNE116005:2012 standard [32]. The dimensions for the design are detailed in Fig. 6.

For the compression specimens, the design established by the UNE-ISO 604:2003 standard [33] is followed, printing a solid cylinder (Fig. 7) with a diameter of 12 mm and a height of 18 mm. For the compression tests, the methodology described by Maćkowiak et al. [34] is followed.

For the flexural test, a specimen was designed to comply with the recommendations of EN-ISO 178:2020 [35]. Fig. 8 shows the dimensions of the specimen used in this article.

However, as indicated above, when using the multifilament printer, the specimens must be redesigned to accommodate different materials. We chose to redesign the specimens in the form of a box so that the outer perimeter of the specimen is made of one material and the inner part or "core" is made of another material. The core is the area that will have mainly the gyroid pattern. This is all done in a CAD design program and then the zones are assigned to the materials in the printer's slicing program.

Fig. 9(a and b) shows a representation of this proposal for the tensile specimen. It distinguishes between the outer material and the inner material with a perimeter of 2 mm on the walls as a box.

For the compression specimens, as in the tensile specimens, it has been necessary to make a new design where one material will go

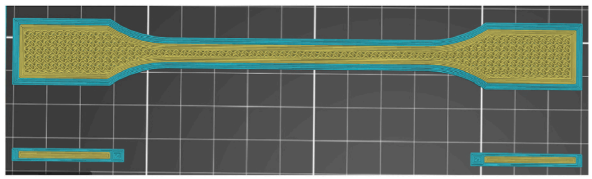

Fig. 2. Application of Gyroid in bed aligned position.

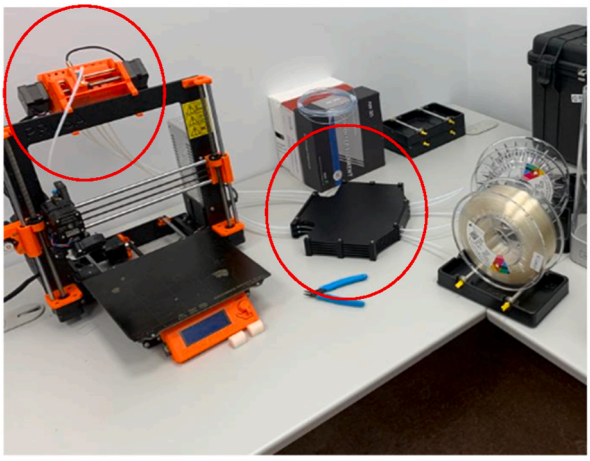

Fig. 3. MK3S & M3S + MMUS printer material distribution system.

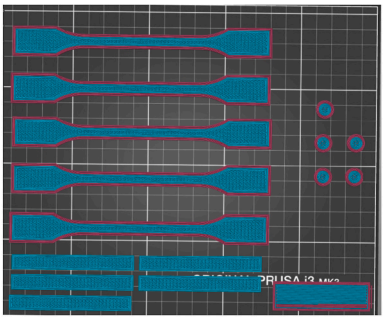

Fig. 4. Specimens and deposition tower in slicing software.

Fig. 5. Prusa i3 MK2S single filament printer.

inside and the other will cover it superficially (Fig. 10). Therefore, the inner material will form a cylinder of radius 4 mm and a height 18 mm while the outer material will have an outer radius of 6 mm and an inner radius of 4 mm and will have the same height as in the case of single specimens. Two lids have been placed so that the same material is in contact with the hot bed.

For the bending specimen, its design is more complicated due to its small dimensions, so the same approach as with the other two specimens is not possible. Therefore, it is designed as a sandwich structure to separate the materials (Fig. 11).

The combinations of tests performed are 16, since all 4 materials are mixed and those specimens that will be of a single material.

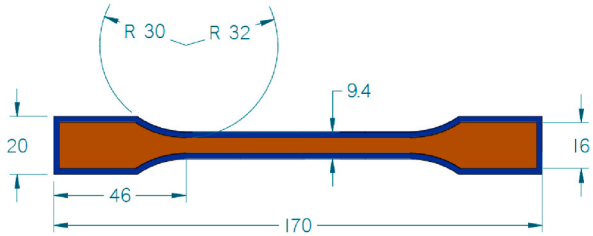

Fig. 6. Specification measurements (mm) for specimen with various tensile materials.

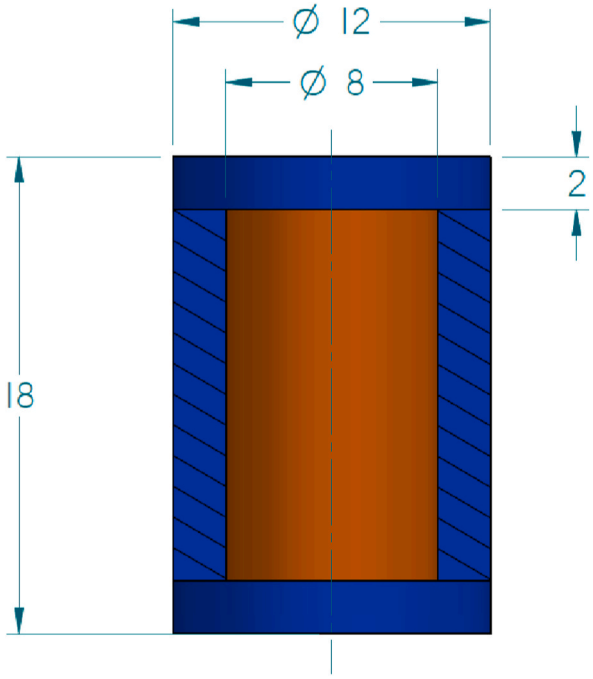

Fig. 7. Specification measurements (mm) for compression specimen with mixed materials.

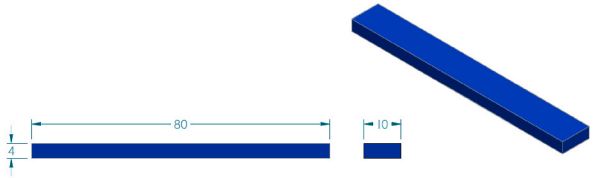

Fig. 8. Specification measurements (mm) for flexural specimen, where units are in mm.

Table 2 identifies all the combinations performed.

The nomenclature used to distinguish the composition of the specimen materials is shown in Fig. 12. The first material denotes the exterior followed by the material composing the core of the specimen.

d. Sample size

The number of samples necessary for the data to be representative and to be able to characterize the materials used is established. For this purpose, a statistical study of the results obtained from the tensile test of a batch of samples printed in PLA has been carried out. In order to set the number of specimens for each batch, the UNE 116005:2012 standard [32] is applied, where it is specified that at least 5 specimens must be used for each test configuration. This sample size value is consistent with that obtained with the usual formulas for sample size calculation, equation (1) [36]. Table 3 shows the values of the parameters used.

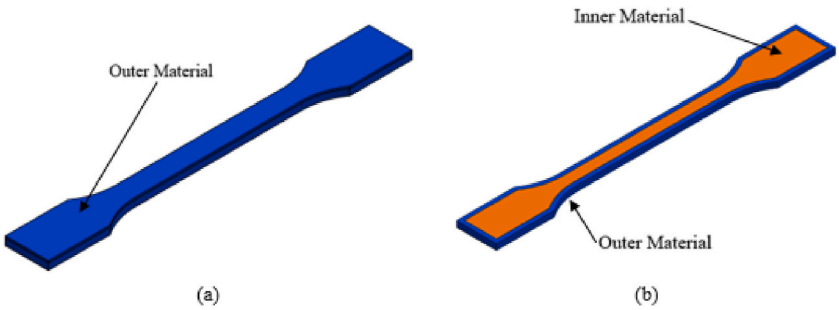

Fig. 9. Tensile test specimen. a) identification of cover. b) identification of materials.

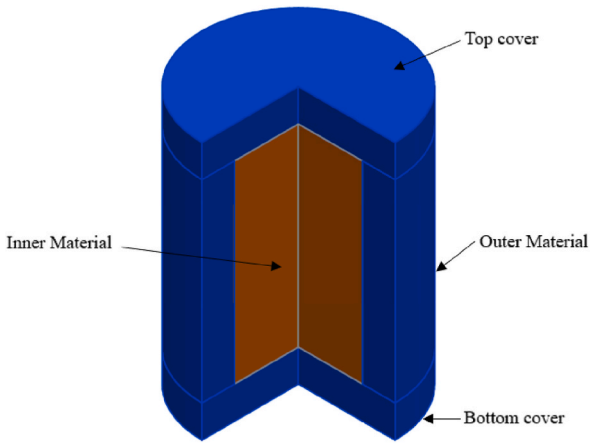

Fig. 10. Compression test specimen with distinction of materials and covers.

Fig. 11. Measured specification for flexural specimen with various materials, where units are in mm.

Table 2
Combinations of filaments.

CONFIGURATION	MATERIALS
I	PLA
II	ABS
III	ASA
IV	PETG
V	PLA-ABS-PLA
VI	PLA-ASA-PLA
VII	PLA-PETG-PLA
VIII	ABS-PLA-ABS
IX	ABS-ASA-ABS
X	ABS-PETG-ABS
XI	ASA-PLA-ASA
XII	ASA-ABS-ASA
XIII	ASA-PETG-ASA
XIV	PETG-PLA-PETG
XV	PETG-ABS-PETG
XVI	PETG-ASA-PETG

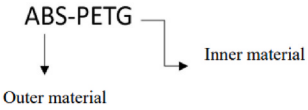

Fig. 12. Example of specimen nomenclature.

$$n = \frac{z^2 \bullet \delta^2}{e} \tag{1}$$

where z is obtained from the standard normal distribution for a confidence level of 95 %, δ is the standard deviation of the population, and e is the acceptable limit of sampling error. To determine the standard deviation, 9 tensile tests were performed with PLA specimens (Fig. 13).

Table 4 shows the results obtained from the 9 tensile specimens:

Once the values are obtained, and substituting in equation (1), it is obtained that the minimum sample size should be 3.84 samples. This value is conservatively close to 5 as indicated by the recommendations of the standard [32,36].

3. Results and discussion

Five tensile specimens were tested for each of the 16 material combinations described in Table 2. In other words, 80 tensile tests were carried out, and the same number of compression and flexural tests were performed to complete a total of 240 tests carried out in the Mechanical Engineering Laboratory of the Universidad Carlos III de Madrid.

3.1. Tensile test results

The Interface 1210ACK-2.5 load cell with a load capacity of up to 50 KN (Fig. 14) and a MEL M1L/100 laser position sensor are used for tensile tests. The test speed is set at 3.5 mm/min according to the recommended test speed according to UNE-EN-ISO 527–1:2020 [37].

The specimens used in the tests are identified as follows: first the outer perimeter material, second the core material, percentage of infill and finally the specimen number. An example of identification is shown in Fig. 15(a and b). All specimens are tested until failure is reached.

The calculations to be performed once the tests have been carried out as detailed in the standards are as follows:

Tensile stress, equation (2), σ_t: Where F is the applied force and A is the cross-sectional area.

$$\sigma_t = \frac{F}{A} \tag{2}$$

Deformation, equation (3), ε: Taking into account the initial length and the elongation undergone.

$$\varepsilon = \frac{\Delta L_0}{L_0} \tag{3}$$

Young's modulus, equation (4), E: The ratio between stress σ_t and strain ε.

$$E = \frac{\sigma_t}{\varepsilon} \tag{4}$$

Table 5 shows, as an example, the results obtained in one of the proposed combinations (outer PETG and inner PLA). Once the parameters of each of the tests are calculated, a stress-strain graph is plotted to observe the behavior of each specimen (Fig. 16).

Figs. 17 and 18 show the maximum value of tensile stress and Young's modulus for all tested combinations. Both figures also show the standard deviation of the five samples tested. It is observed that the highest standard deviations are obtained with the combination of materials, while the tests of homogeneous specimens without mixture show less dispersion with results closer to their corresponding means. This behavior of the standard deviation is consistent with the study by Baca et al. [38] that obtains similar standard deviations in sandwich type specimens.

Table 6 shows the results of the tensile tests presented as the average of the 5 specimens manufactured for each combination. The

Table 3
Sample size calculation parameters.

Parameters for sample size calculation:	
Maximum acceptable error:	5 %
Estimated percentage of the sample:	50 %
Desired level of confidence:	95 %
Value of z	1.96
Acceptable limit of sampling error e	5 %

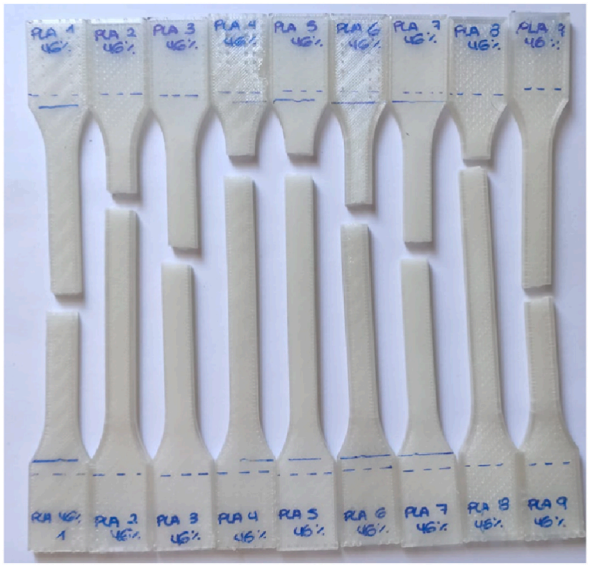

Fig. 13. Samples used to determine sample size.

Table 4
Test results with the pilot specimen

Test number	Maximum stress (MPa)
1	27.643
2	33.582
3	28.718
4	29.268
5	27.799
6	31.046
7	27.788
8	29.386
9	32.927
AVERAGE	29.796
STANDARD DEVIATION	2.235

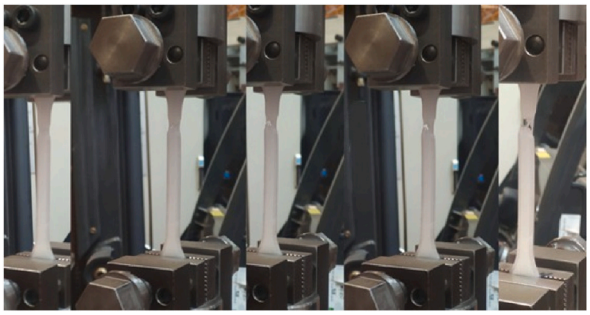

Fig. 14. Interface 1210ACK-2.5 tensile testing machine.

best mechanical properties are obtained with the PETG-PLA combination, which has a tensile strength of 43.8 MPa, a strain of 0.0387 and a Young's modulus of 1.68 GPa. The comparison with the symmetrical combination, i.e. PLA on the outside and PETG on the inside, shows a significant reduction in mechanical properties: tensile strength of 32.2 MPa and Young's modulus of 1.57 GPa. The authors consider that this difference in behavior is due to the fact that PLA is a much stiffer material than PETG and therefore, when it acts as the core of the specimen together with the gyroid pattern, it provides greater resistance.

Another interesting conclusion that can be drawn from Figs. 17 and 18 is that multi-material specimens have better mechanical behavior than homogeneous specimens.

(a) (b)

Fig. 15. (a) Tensile specimens. (b) Specimen labeling.

Table 5
Tensile test results for the PETG-PLA combination.

	PLA-ABS				
	PETG-PLA 1	PETG-PLA 2	PETG-PLA 3	PETG-PLA 4	PETG-PLA 5
Maximum force (N)	1623	1696	1857	1775	1809
Displacement (mm)	4.84	3.89	4.86	4.78	4.84
Maximum stress (MPa)	40.58	42.41	46.42	44.38	45.23
E (Gpa)	1.504	1.643	1.739	1.693	1.809
σ (MPa) (average)			43.8		
ε (mm/mm) (average)			0.0387		
E (Gpa) (mean)			1.678		

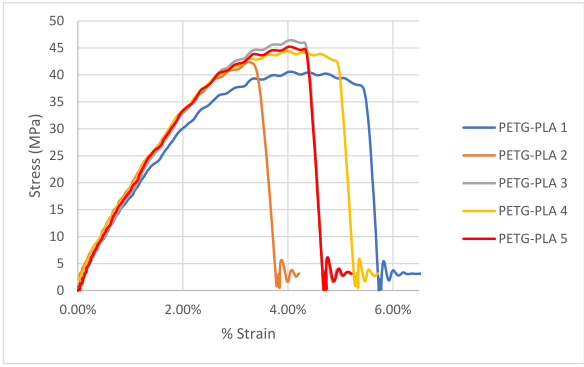

Fig. 16. Stress (MPa) vs. strain curve for PETG-PLA in tensile test.

3.2. Compression test results

A representative image of the type of specimens used in compression tests is shown in Fig. 19.

The compression tests were performed with MicroTest equipment (see Fig. 20(a and b)) with a load cell of up to 50 kN in order to move a moving head and thus exert compressive force on the specimen. The test was performed at a speed of 10 mm/min, following the recommendation of the standard [33].

The calculations performed after the compression tests are as follows:

Compressive stress, equation (5), σ_c: The force exerted on the cross-sectional area.

$$\sigma_c = \frac{F}{A} \tag{5}$$

Deformation in compression, equation (6), ε_c: Taking into account the deformation suffered between the initial length.

$$\varepsilon_c = \frac{\Delta L_0}{L_0} \tag{6}$$

Young's modulus equation (7), E: The ratio between stress and strain.

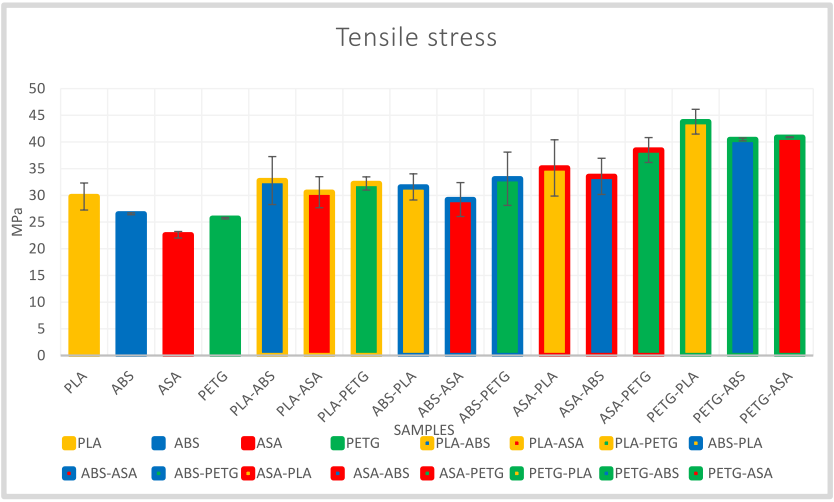

Fig. 17. Maximum stress results in the tensile test.

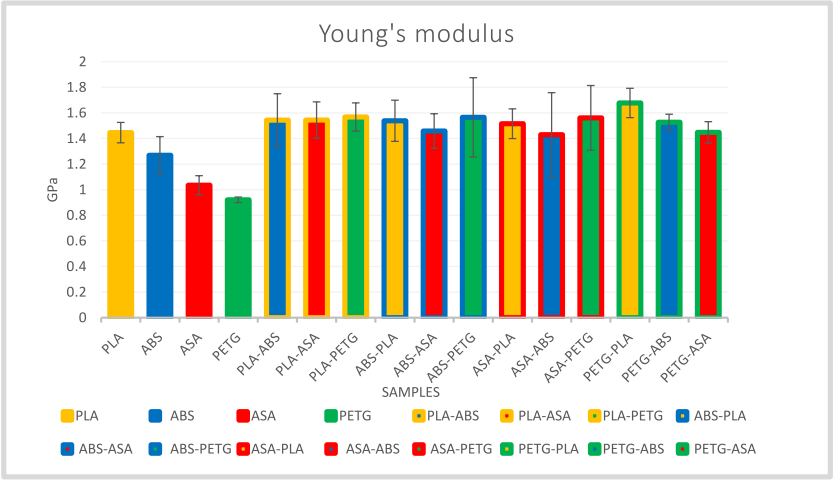

Fig. 18. Young's modulus results in the tensile test.

Table 6
Tensile test results.

COMBINATIONS	MAXIMUM TENSILE STRENGTH (MPa)	YOUNG'S MODULE (GPa)
PLA	29.785	1.446
ABS	26.543	1.269
ASA	22.619	1.035
PETG	25.722	0.9209
PLA-ABS	32.774	1.5436
PLA-ASA	30.591	1.5443
PLA-PETG	32.229	1.5681
ABS-PLA	31.582	1.5385
ABS-ASA	29.219	1.4585
ABS-PETG	33.114	1.5655
ASA-PLA	35.14	1.5155
ASA-ABS	33.561	1.4299
ASA-PETG	38.495	1.5611
PETG-PLA	43.803	1.6776
PETG-ABS	40.475	1.5271
PETG-ASA	40.891	1.448

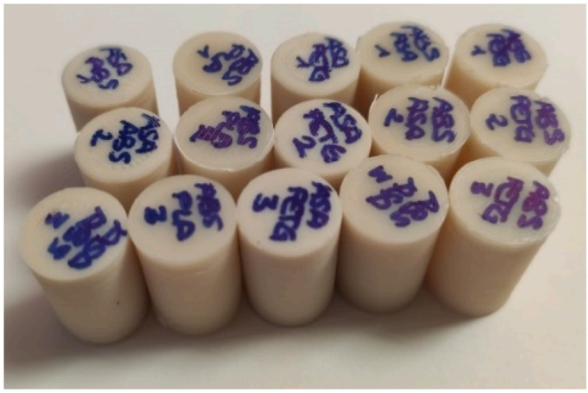

Fig. 19. Compression specimens.

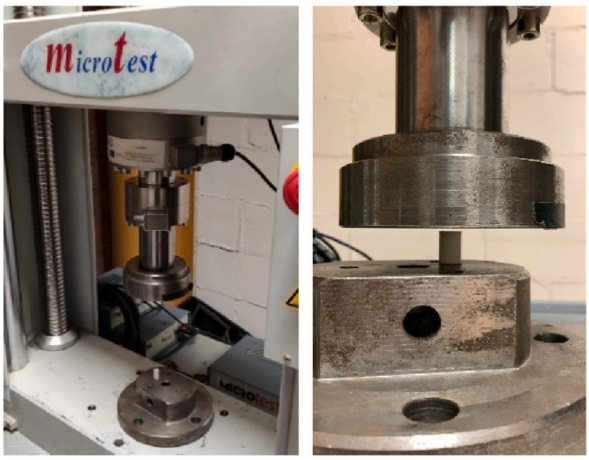

Fig. 20. (a) Microtest machine for compression test. (b) Specimen test.

$$E = \frac{\sigma_c}{\varepsilon} \tag{7}$$

Table 7 shows, as an example, the results obtained for the combination of materials with the highest compressive strength. This is the PLA-ABS combination. Fig. 21 shows the stress-strain graph for the five tested specimens of this configuration.

Figs. 22 and 23 show the maximum values of compressive stress and Young's modulus for all tested combinations. The best results are obtained with the PLA-ABS material combination with a maximum compressive stress of 54.7 MPa and Young's modulus of 1.59 GPa. Another conclusion that can be drawn from Figs. 22 and 23 and Table 8 is that the mechanical properties are very similar in those combinations where PLA is used as the outer material of the specimen. The authors consider that this behavior is again determined by the stiffer characteristics of PLA compared to the other materials. As in the tensile tests, it is observed that the comparison with the symmetrical combinations, i.e. PLA inside the specimen, shows a significant reduction of the mechanical properties. The results

Table 7
Compression test results for the PLA-ABS combination.

	PLA-ABS				
	PLA-ABS 1	PLA-ABS 2	PLA-ABS 3	PLA-ABS 4	PLA-ABS 5
Maximum force (N)	6230	6210	6120	6220	6180
Displacement (mm)	1.0	0.67	0.85	0.87	0.799
Maximum stress (MPa)	55.085	54.908	54.112	54.996	54.643
E (Gpa)	1.649	1.505	1.667	1.621	1.572
σ (MPa) (average)			54.749		
ε (mm/mm) (average)			4.654		
E (Gpa) (mean)			1.597		

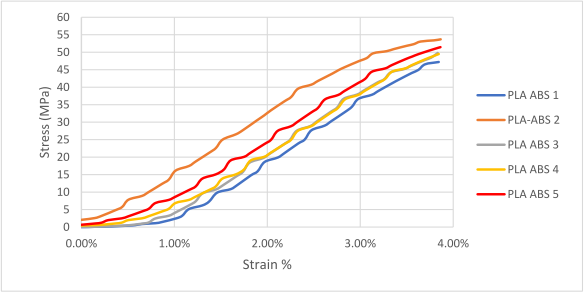

Fig. 21. Compression test stress-strain graph of PLA-ABS combination.

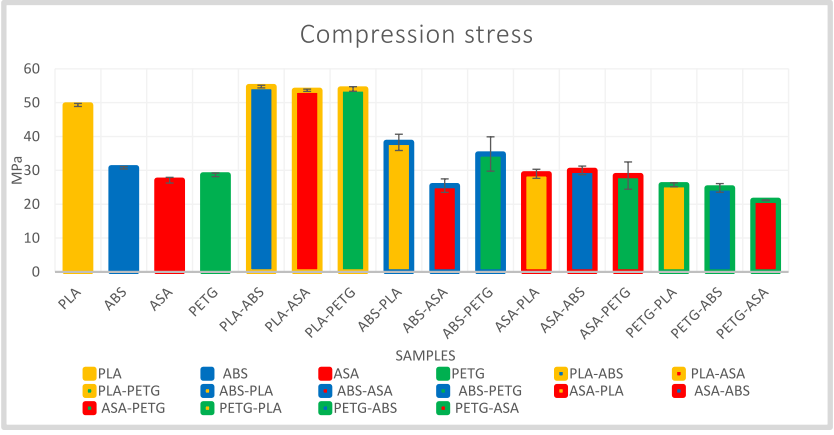

Fig. 22. Results of maximum compressive stress.

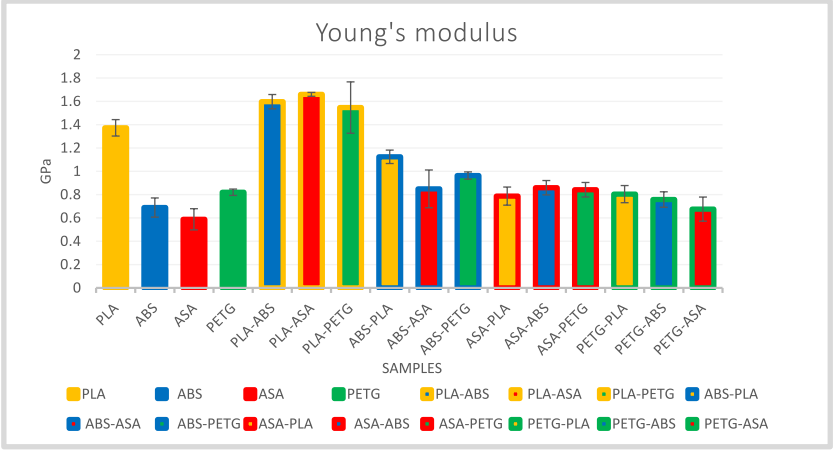

Fig. 23. Young's modulus results for the compression test.

obtained for maximum stress when PLA is used as the outer material of the specimen are of the same order of magnitude as the maximum stress of the material, i.e. they are in the range of 48–61 MPa. This conclusion is consistent with other authors as Gao et al. [39].

The dispersion of the results is very low, apart from the ABS-PETG and ASA-PETG combination, which allows to conclude that the results are robust and with low variability.

Another conclusion that can be drawn from Figs. 22 and 23 is that materials with greater flexibility, such as PETG, worsen the mechanical compressive strength of the parts when they are used on the outside of the parts and directly exposed to the load. These materials improve the compressive behavior of the parts when used as core material. This statement contrasts with the results obtained

Table 8
Compression test results.

COMBINATIONS	MAXIMUM TENSILE STRENGTH (MPa)	YOUNG'S MODULE (GPa)
PLA	49.3203	1.37288
ABS	30.77	0.6892
ASA	27.0917	0.5882
PETG	28.6656	0.8202
PLA-ABS	54.7493	1.59708
PLA-ASA	53.6529	1.65976
PLA-PETG	54.0419	1.54672
ABS-PLA	38.2679	1.1242
ABS-ASA	25.4825	0.8492
ABS-PETG	34.8372	0.9635
ASA-PLA	28.9795	0.7872
ASA-ABS	29.9919	0.8592
ASA-PETG	28.4534	0.8418
PETG-PLA	25.7477	0.8042
PETG-ABS	24.8105	0.758
PETG-ASA	21.1499	0.6756

in traction where the best mechanical properties are obtained with PETG as the outer material and PLA as the core.

From the results of the compression tests, it can be concluded that stiffer materials improve the mechanical properties when located on the outside of the specimen. It can also be concluded that the multi-material specimens have a slightly improved mechanical behavior compared to the homogeneous specimens.

3.2.1. Bending test results

The bending test is performed according to UNE-EN-ISO 178:2020 [35]. For this test, a manually operated machine with a 1000 kg load cell, Sensocar model S2-A, is used. The force is applied by means of a punch as shown in Fig. 24.

The calculations to be performed once the tests have been carried out as detailed in the standards [35] are as follows:

Bending stress, equation (8), σ_f: where w is the width of the specimen, h the thickness, L the length and F the force exerted.

$$\sigma = \frac{M \bullet c}{I} = \frac{3FL}{2wh^2} \tag{8}$$

Deformation in bending, equation (9), ε_f: The deflection, thickness h and length L are taken into account. δ, the thickness h and the length L are considered.

$$\varepsilon_f = \frac{6\delta h}{L^2} \tag{9}$$

Flexural modulus, equation (10), E: The ratio between stress and strain.

$$E = \frac{L^3 F}{4wh^3\delta} \tag{10}$$

Table 9 shows, as an example, the results obtained for the combination of materials that obtains the maximum flexural strength. These are homogeneous PLA specimens. This is a notable difference with the compression and tensile tests, i.e. in bending the

Fig. 24. Machine for bending test.

homogeneous specimens obtain better mechanical properties than the combined specimens. Once the parameters of each of the tests are calculated, the stress-strain graph is made to observe the behavior of each specimen (Fig. 25).

Figs. 26 and 27 show the maximum flexural strength and Young's modulus achieved by the combinations tested in flexure. Table 10 shows all the results from this test. Contrary to the tensile and compression tests, the maximum value is obtained for a homogeneous blend, PLA, with a maximum bending stress of 21.046 MPa and a Young's modulus of 0.72 GPa. A first analysis of the results of the bending tests indicates that the configuration of the specimens, sandwich type, fixed by the test standard is not the most suitable for the combination of materials. This conclusion can be extracted by comparing the results of the compression and tensile tests where the specimens that were combined with PLA on the outside have better mechanical properties. The authors consider that a possible explanation for these results is that the sandwich configuration is more prone to adhesion problems between the different materials that compose it, as shown in Fig. 28, unlike the tensile and compression test specimens in which one material is completely covered inside the other. On the other hand, it is also observed that those materials that have a better bonding compatibility in the impression, as is the case of PETG-PLA, present good mechanical properties obtaining the second highest results in the maximum flexural strength (17.14 MPa) and one of the highest values of the flexural modulus (0.436 GPa). This combination of PETG-PLA materials is the one that obtains the best mechanical results in tensile tests.

As for the other combinations of materials, it can be concluded that the stiffer materials perform worse than those with greater flexibility.

In view of the results of the bending test, the authors consider that the dimensions of the specimens according to the current test standard UNE-EN-ISO 178:2020 [35] are a limitation to investigate the improvement of behavior by combining materials. The specimens indicated in the standard are only 4 mm thick and taking into account the resolution of the fused deposition modeling printers, they present adhesion problems that do not allow the contribution of several materials to be adequately assessed.

The dimensions of the bending specimen do not allow the proposed configuration to be used in the other two types of tests without breaking regulations. Although the sandwich configuration is interesting for the study of the combination of materials, the adhesion between layers is reduced and it is prone to stress concentrators and easy separation, which does not make it viable for stresses in other directions than that of the fibers of the part. By using a core material and an outer material, a wall effect is achieved that distributes stresses more efficiently across the printing parameters of the part.

4. Conclusions

This study presents the mechanical properties derived from combining various materials using fused deposition modeling (FDM) 3D printing. Utilizing a gyroid printing pattern, 240 specimens were fabricated to evaluate mechanical strength and Young's modulus through tensile, compression, and flexural tests. The specimens were uniformly printed using PLA, PETG, ASA, and ABS, with additional specimens combining two of these materials. The selection criteria for these materials were their accessibility and common usage in the 3D printing industry. All specimens were manufactured and tested according to the applicable UNE standards for each type of test.

The experimental results yield the following conclusions:

- No single material combination dominated across all three types of tests.
- In tensile testing, the combination of PETG as the outer material with PLA in the core exhibited the best mechanical properties, achieving a tensile strength of 43.8 MPa and a Young's modulus of 1.68 GPa.
- In compression testing, the combination of PLA as the outer material with ABS in the core showed superior mechanical properties, with a compressive strength of 54.7 MPa and a Young's modulus of 1.59 GPa.
- In flexural testing, homogeneous PLA specimens displayed the best mechanical properties, with a maximum bending stress of 21.046 MPa and a Young's modulus of 0.72 GPa.
- Among the four materials tested, PLA consistently demonstrated the best mechanical properties. The optimal performance of PLA varied with its position: it performed better in tensile tests when placed in the core and in compression tests when positioned on the outside.

Table 9
Results of flexural tests with PLA.

	PLA				
	PLA 1	PLA 2	PLA 3	PLA 4	PLA 5
Maximum force (N)	37.5	32	31	35	35
Displacement (mm)	8.75	7	8.75	10.5	10.5
Maximum stress (MPa)	23.13	19.74	19.123	21.59	21.59
E (GPa)	0.82669	0.82669	0.71541	0.66452	0.57233
σ (MPa)			21.0346		
ε (mm/mm)			0.0504		
E (GPa)			**0.7211**		

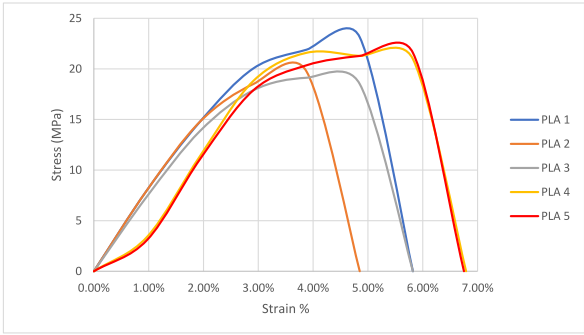

Fig. 25. Bending test results homogeneous PLA configuration.

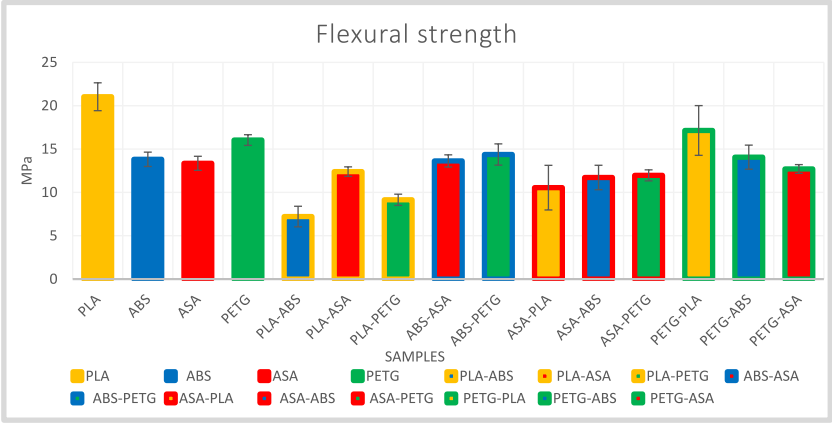

Fig. 26. Results of the maximum stress in flexural test.

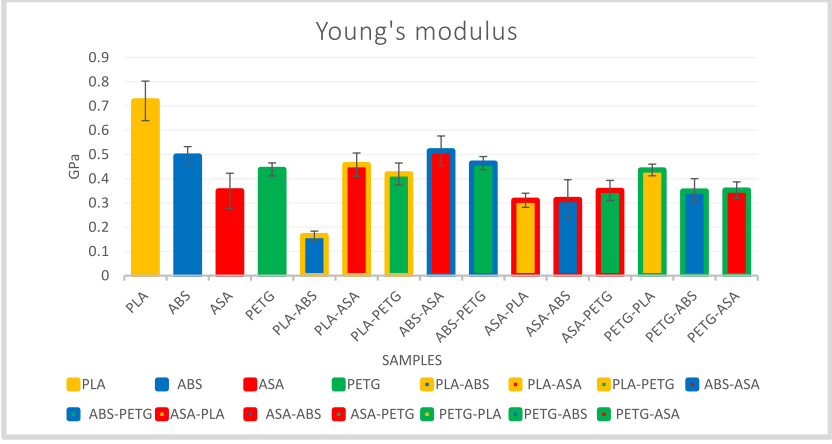

Fig. 27. Young's modulus results in flexural test.

- The printing parameters utilized in this research effectively determined the mechanical properties of the specimens. The gyroid pattern proved capable of tolerating high loads and provided behavior similar to 100 % density printing, despite using less material as all specimens were printed at 46 % density.

This study confirms that material combinations in additive manufacturing offer a viable solution for enhancing the mechanical properties of printed parts, analogous to the role metallic alloys have played in metal development.

Additionally, this research identified a limitation in the standard dimensions for flexural test specimens. With a thickness of only 4

Table 10
Results of bending tests.

COMBINATIONS	MAXIMUM BEND STRENGTH (MPa)	YOUNG'S MODULE (GPa)
PLA	21.0346	0.7211
ABS	13.81754	0.4934
ASA	13.3558	0.3498
PETG	16.0386	0.4381
PLA-ABS	7.2152	0.1653
PLA-ASA	12.398	0.4579
PLA-PETG	9.1486	0.4197
ABS-ASA	13.6298	0.5151
ABS-PETG	14.3729	0.4642
ASA-PLA	10.55012	0.311
ASA-ABS	11.7202	0.3141
ASA-PETG	11.9676	0.3515
PETG-PLA	17.1438	0.436
PETG-ABS	14.0636	0.3491
PETG-ASA	12.7056	0.3529

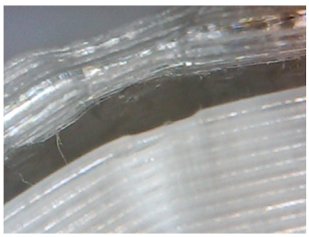

Fig. 28. Example of poor adhesion between materials during flexural testing.

mm, the potential for testing material combinations is significantly constrained.

As future work, the authors consider that it would be interesting to quantify the effect of the use of compatibilizers to improve the compatibility between ABS and PETG.

CRediT authorship contribution statement

Ana María Gómez Amador: Writing – review & editing, Writing – original draft, Resources, Methodology, Investigation, Formal analysis, Data curation, Conceptualization. **Ricardo Andre Venturini Avendano:** Writing – review & editing, Writing – original draft, Methodology, Investigation, Formal analysis, Data curation. **Alejandro Quesada González:** Writing – review & editing, Methodology, Formal analysis, Data curation. **Leopoldo Prieto Fernández:** Writing – review & editing, Writing – original draft, Investigation, Formal analysis.

Data and code availability

Data will be made available on request. For requesting data, please write to the corresponding author.

Declaration of competing interest

The authors declare that they have no known competing financial interests or personal relationships that could have appeared to influence the work reported in this paper.

Acknowledgements

This work has been developed in the Mechanical Laboratory at Universidad Carlos III de Madrid.

References

[1] S. Crump, Fast, Precise, Safe Prototype with FDM, ASME PED vol. 50, 1991, pp. 53–60. https://utw10945.utweb.utexas.edu/Manuscripts/1991/1991-15-Wales.pdf. (Accessed 7 August 2022).
[2] M. Placek, "Top 3D printing technologies 2021. Statista.," [Online]. Available: https://www.statista.com/statistics/560304/worldwide-survey-3d-printing-top-technologies/. [Accessed 2022 August 7].
[3] S. Beyerlein, M. Aboushama, Evaluation of Continuous Fiber Reinforcement Desktop 3D Printers: Desktop 3D Printers Overview, 2020.

[4] M. Doshi, M. Ameya, S. Kumar, S. Deshmukh, Printing parameters and materials affecting mechanical properties of FDM-3D printed parts: perspective and prospects, Mater. Today Proc. 50 (2022) 2269–2275.
[5] S. Anoop Kumar, R. Ohdar, S. Mahapatra, Parametric appraisal of mechanical property of fused deposition modelling processed parts, Mater. Des. 31 (1) (2010) 287–295.
[6] J.R. Lennert, J. Sárosi, Investigation of 3D printing parameters affecting the impact strength, Int. J. Eng. XIX (2021).
[7] B. Akhoundi, A. Behravesh, Effect of filling pattern on the tensile and flexural mechanical properties of FDM 3D printed products, Exp. Mech. 59 (6) (2019) 883–897.
[8] M.A. Caminero, J.M. Chacón, E. García-Plaza, P.J. Nuñez, J.M. Reverte, J.P. Becar, Additive manufacturing of PLA-based composites using fused filament fabrication: effect of graphene nanoplatelet reinforcement on mechanical properties, Polymers 11 (5) (2019) 799. https://doi.org/10.3390/polym11050799.
[9] Smart materials 3D, PLA technical data sheet," [Online]. Available: https://www.smartmaterials3d.com/pla. [Accessed 15 January 2025].
[10] PLA, Polylactic Acid: The Environmentally Friendly Plastic," [Online]. Available: https://descubrearduino.com/que-es-pla/. [Accessed 15 January 2015].
[11] Smart materials 3D. ABS Technical Data Sheet," [Online]. Available: https://www.smartmaterials3d.com/abs-filamento. [Accessed 15 January 2025].
[12] S. Raam, S. Sridhar, R. Venkatraman, M. Venkatesan, Polymer additive manufacturing of ASA structure: influence of printing parameters on mechanical properties, Mater. Today Proc. 39 (2021) 1316–1319.
[13] L. Yuan, S. Ding, C. Wen, Additive manufacturing technology for porous metal implant applications and triple minimal surface structures: a review, Bioact. Mater. 4 (2018) 56–70.
[14] J. Otero, A. Vijverman, M. Mommaerts, Use of fused deposit modeling for additive manufacturing in hospital facilities: European certification directives, J. Cranio-Maxillofacial Surg. 45 (2017) 1542–1546.
[15] Multi-Material 3D Printer: Types & Printing Guide. All3DP," [Online]. Available: https://all3dp.com/2/multi-material-3d-printing-an-overview/. [Accessed 15 January 2025].
[16] A. Bandyopadhyay, K.D. Traxel, S. Bose, Nature-inspired materials and structures using 3D Printing, Mater. Sci. Eng. R Rep. 145 (2021).
[17] J. Jiang, Y. Xiong, Z. Zhang, D.W. Rosen, Machine learning integrated design for additive manufacturing, J. Intell. Manuf. 22 (2022) 1073–1086.
[18] T. Xiaoyong, L. Tengfei, Y. Chuncheng, W. Qingrui, L. Dichen, Interface and performance of 3D printed continuous carbon fiber reinforced PLA composites, Compos. Appl. Sci. Manuf. 88 (2016) 198–205.
[19] J. Schweiger, F. Beuer, M. Stimmelmayr, D. Edelhoff, P. Magne, J.F. Güth, Histo-anatomic 3D printing of dental structures, Br. Dent. J. 221 (9) (2016) 555–560.
[20] J. An, K.F. Leong, Multi-material and multi-dimensional 3D printing for biomedical materials and devices, Biomedical Materials & Devices 1 (2023) 38–48.
[21] B. Yermurat, Ö. Seçgin, V. Taşdemir, Multi-material additive manufacturing: investigation of the combined use of ABS and PLA in the same structure, Mater. Test. 65 (7) (2023) 1119–1126.
[22] Understanding the Gyroid Infill in 3D Printing," Wevolver, [Online]. Available: https://www.wevolver.com/article/gyroid-infill. [Accessed 15 January 2025].
[23] Z. Qin, G.S. Jung, M.J. Kang, M.J. Buehler, The mechanics and design of a lightweight three-dimensional graphene assembly, Sci. Adv. 3 (1) (2017), https://doi.org/10.1126/sciadv.1601536.
[24] R. Vrana, D. Koutny, D. Palousek, Impact resistance of different types of lattice structures manufactured by SLM, MM Science Journal (December 2016), https://doi.org/10.17973/MMSJ.2016_12_2016186.
[25] Y. Nian, S. Wan, M. Avcar, R. Yue, M. Li, 3D printing functionally graded metamaterial structure: design, fabrication, reinforcement, optimization, Int. J. Mech. Sci. 258 (2023).
[26] D. Bell, T. Siegmund, 3D-printed polymers exhibit a strength size effect, Addit. Manuf. 21 (2018) 658–665.
[27] D.W. Abueidda, M. Bakir, R.K.A. Al-Rub, J.S. Bergström, N.A. Sobh, I. Jasiuk, Mechanical properties of 3D printed polymeric cellular materials with triply periodic minimal surface architectures, Mater. Des. 122 (2017) 255–267.
[28] D.W. Abueidda, M. Elhebeary, C.-S.(Shiang, S. Pang, R.K.A. Al-Rub, I.M. Jasiuk, Mechanical properties of 3D printed polymeric Gyroid cellular structures: experimental and finite element study, Mater. Des. 165 (2019).
[29] C. Silva, A.I. Pais, G. Caldas, B.P.P.A. Gouveia, J.L. Alves, J. Belinha, Study on 3D printing of gyroid-based structures for superior structural behaviour, Progress in Additive Manufacturing 6 (2021) 689–703.
[30] G. Ćwikła, C. Grabowik, K. Kalinowski, I. Paprocka, P. Ociepka, The influence of printing parameters on selected mechanical properties of FDM/FFF 3D-printed parts, IOP Conf. Ser. Mater. Sci. Eng. 227 (2017).
[31] A. Lanzotti, M. Grasso, G. Staiano, M. Martorelli, The impact of process parameters on mechanical properties of parts fabricated in PLA with an open-source 3-D printer, Rapid Prototyp. J. 21 (2015) 604–617.
[32] UNE 116005:2012. Manufacturing by additive of caps on plastics. Additive manufacturing. Preparation of test pieces," UNE Normalización Española. [Online]. [Accessed 15 January 2025].
[33] UNE-EN ISO 604:2003 Plastics - Determination of compressive properties," UNE Normalización Española. [Online]. [Accessed 15 January 2025].
[34] P. Maćkowiak, D. Płaczek, M. Kotyk, Determination of design mechanical properties of adhesives in a tensile and compression test, IOP Conf. Ser. Mater. Sci. Eng. 393 (2018).
[35] UNE-EN ISO 178:2020 Plastics - Determination of flexural properties," UNE Normalización Española. [Online]. [Accessed 15 January 2025].
[36] G.I. Pacheco, Tensile Analysis of 3D Printed Specimens by Fused Wire Deposition of PLA, ABS and PLA/MLO, Universidad Politécnica Salesiana de Cuenca, 2019.
[37] UNE-EN ISO 527-1:2020 Plastics - Determination of Tensile Properties - Part 1: General Principles," UNE Normalización Española. [Online]. [Accessed 15 January 2025].
[38] D.M. Baca Lopez, R. Ahmad, Tensile mechanical behaviour of multi-polymer sandwich structures via fused deposition modelling, Polymers 12 (2020).
[39] G. Gao, F. Xu, J. Xu, Z. Liu, Study of material color influences on mechanical characteristics of fused deposition modeling parts, Materials 15 (2022).